Paramagnetism and antiferromagnetic interactions in Cr-doped GaN

2011 J. Phys.: Condens. Matter 23 346004

(http://iopscience.iop.org/0953-8984/23/34/346004)

IOP PUBLISHING JOURNAL OF PHYSICS: CONDENSED MATTER

J. Phys.: Condens. Matter **23** (2011) 346004 (9pp) doi:10.1088/0953-8984/23/34/346004

Paramagnetism and antiferromagnetic interactions in Cr-doped GaN

L M C Pereira[1,2,3], T Som[1,4], J Demeulemeester[1], M J Van Bael[5], K Temst[1] and A Vantomme[1]

[1] Instituut voor Kern- en Stralingsfysica and INPAC, K U Leuven, 3001 Leuven, Belgium
[2] IFIMUP and IN-Institute of Nanoscience and Nanotechnology, Faculdade de Ciências da Universidade do Porto, 4169-007 Porto, Portugal
[3] Instituto Tecnológico e Nuclear, UFA, 2686-953 Sacavém, Portugal
[4] Institute of Physics, Bhubaneswar 751005, Orissa, India
[5] Laboratory of Solid-State Physics and Magnetism and INPAC, K U Leuven, 3001 Leuven, Belgium

E-mail: linomcp@fc.up.pt

Received 8 June 2011, in final form 14 July 2011
Published 12 August 2011
Online at stacks.iop.org/JPhysCM/23/346004

Abstract

We report on the magnetic and structural properties of Cr-doped GaN prepared by ion implantation of epitaxial thin films. Based on a detailed analysis of the magnetometry data, we demonstrate that the magnetic interactions between Cr moments in GaN are antiferromagnetic (AFM). Increasing the Cr fractional concentration up to 0.35, we observe that strong nearest cation neighbor AFM coupling results in the reduction of the effective moment per Cr atom. The uncompensated Cr moments exhibit paramagnetic behavior and we discuss to what extent the effects of an anisotropic crystal field and AFM interactions can be inferred from the magnetization data. We discuss the observed changes in magnetic and structural properties induced by thermal annealing in terms of defect annealing and Cr aggregation.

1. Introduction

Over the past decade, the magnetism of wide-gap semiconductors doped with 3*d* transition metals, or dilute magnetic semiconductors (DMS), has become one of the most controversial topics in condensed matter physics. Despite the remarkable volume of experimental and theoretical research and significant developments in synthesis and characterization methods, the origin of high-temperature ferromagnetism in wide-gap DMS remains far from consensual [1].

Soon after the first report on Co-doped TiO_2 [2], ferromagnetism at and above room temperature was reported in many other wide-gap DMS materials (cf, e.g. the reviews [3–6]). Research in the ensuing years followed two main directions, the search (i) for new DMS materials displaying signatures of high-temperature ferromagnetic order (e.g. Gd-doped GaN [7], C-doped ZnO [8], and undoped HfO_2 [9]) and (ii) for the origin and control of ferromagnetism in those systems regarded as most attractive (e.g. Co- and Mn-doped ZnO [10] and Mn-doped GaN [11]). However, as the understanding of some of the most intensively studied materials deepened, issues of irreproducibility and instability became common features of these materials. A number of non-intrinsic sources of ferromagnetism were identified and became well documented: magnetic contaminations [12–15], measurement artifacts [13, 14], spinodal decomposition (e.g. in Co-doped ZnO [16]) and secondary-phase formation (e.g. in ZnO doped with Fe, Co and Ni [17–19]). On the other hand, studies on well-characterized DMS materials (single-phase and homogeneous) found only paramagnetism (e.g. in Mn-doped GaN [20] and Co-doped ZnO [21]), antiferromagnetic interactions (e.g. in Mn-doped GaN [22] and in Co-doped ZnO [23–26]), or, at best, ferromagnetic order with very low Curie temperature (e.g. in Mn-doped GaN [11]). Consequently, the current view on wide-gap DMS is moving toward the belief that the often observed high-temperature ferromagnetism may be non-intrinsic [1]. Key to solving this controversy is a systematic and detailed mapping of the type and strength of the magnetic interactions in the most representative combinations of magnetic dopants and wide-gap semiconductor hosts. In this sense, Cr-doped GaN is an interesting case. Although far from being one of the most intensively studied cases, it has accumulated a significant number of reports of

high-temperature ferromagnetism [27–33]. However, while focusing on the intrinsic origin of the observed ferromagnetic signatures by demonstrating the absence of secondary-phase formation, these studies lack a deeper analysis of the magnetic behavior itself.

Transition metals can be incorporated into GaN during growth [27–31] or by ion implantation [32, 33]. The advantage of ion implantation with respect to the production of uniform and single-crystalline DMS nanolayers is that it is less likely to suffer from the formation of secondary phases. Ion bombardment inevitably leads to lattice disorder, a major concern when electrical and optical dopants are introduced by ion implantation [34]. For magnetic doping, however, lattice disorder is believed to be crucial in establishing the ferromagnetic order, in the form of either point [35] or extended [36] defects. Depending on the implantation conditions, different types of defects can be produced in ion-implanted GaN. At the low fluence end, isolated [37] or clustered [38] point defects are typically observed. As the fluence increases, bands of large planar defects are formed parallel to the basal plane of GaN [38]. Ion-implanted DMS materials are thus interesting systems in which to study the interplay between magnetic dopants and lattice defects.

The most straightforward and reproducible parameter to control, in order to tune the amount and type of ion beam damage, is temperature, either during implantation or during subsequent thermal annealing [39]. Typically, the accumulation of stable defects in irradiated semiconductors, which can eventually result in amorphization, can be reduced by increasing the implantation temperature. In GaN, the accumulated damage decreases rather sharply as the irradiation temperature is increased up to 300 °C, and more slowly above that [40]. On the other hand, high fluence ion implantation at elevated temperatures (550 °C) has been reported to induce dramatic erosion of GaN [41]. Implantation temperatures around 300 °C can thus be expected to yield a good compromise between avoiding amorphization and minimizing surface erosion of GaN. Further control over beam-induced damage is typically realized by thermal treatment. Annealing of implantation disorder in GaN is, however, a rather complex problem. The rule of thumb is that temperatures of around two thirds of the melting point (in units of K) are required to remove extended defects in compound semiconductors. For GaN, this corresponds to about 1600 °C, based on its calculated melting point [42]. However, annealing of GaN at such high temperatures is counteracted by material decomposition involving loss of nitrogen from the GaN surface (e.g. [43]). In addition, high-temperature annealing may result in undesired segregation of Cr or CrN secondary phases [44]. Therefore, when studying the magnetism of ion-implanted GaN DMS materials and its dependence on defect concentration, optimum annealing conditions are those providing a significant degree of damage recovery while avoiding surface decomposition and phase segregation.

In this paper, we analyze the magnetic and structural properties of Cr-doped GaN thin films, produced by implanting Cr^+ ions in epitaxial GaN thin films. Covering a wide range of Cr fractional concentrations (0.005–0.35), from the very dilute regime to well above the site percolation threshold (0.20), and focusing on an in-depth analysis of the magnetometry data, we aim at identifying the type of magnetic interactions between Cr moments in GaN. Combined with structural characterization of as-implanted and annealed samples by means of x-ray diffraction (XRD) and Rutherford backscattering and channeling spectrometry (RBS/C), we investigate how the magnetic behavior is influenced by thermal annealing.

Table 1. Sample list. The naming is according to substrate, S for silicon and A for Al_2O_3, and implanted fluence, in units of 1×10^{15} at. cm^{-2}. All implantations were performed at 300 °C.

Name	Substrate	Fluence (at. cm^{-2})	Peak concentration (x_p)
S1	Si	1×10^{15}	0.005
A1	Al_2O_3	1×10^{15}	0.005
S4	Si	4×10^{15}	0.02
A4	Al_2O_3	4×10^{15}	0.02
S10	Si	1×10^{16}	0.05
A10	Al_2O_3	1×10^{16}	0.05
S20	Si	2×10^{16}	0.10
A20	Al_2O_3	2×10^{16}	0.10
S40	Si	4×10^{16}	0.20
A40	Al_2O_3	4×10^{16}	0.20
S70	Si	7×10^{16}	0.35
A70	Al_2O_3	7×10^{16}	0.35

2. Experimental results

2.1. Sample preparation and structural characterization

High-quality epitaxial GaN(0001) thin films were grown by metalorganic vapor phase epitaxy (MOVPE). Two wafers were grown using different substrates: a 2 μm thick GaN(0001) layer on an Al_2O_3(0001) substrate and an 800 nm GaN(0001) layer on a Si(111) substrate using an AlN/AlGaN intermediate layer. Pieces from each of the wafers were implanted at 300 °C with Cr^+ ions with an energy of 80 keV to fluences ranging from 1×10^{15} to 7×10^{16} at. cm^{-2}. The implantations were performed under an angle of 7° with respect to the surface normal in order to minimize ion channeling [45]. Using the TRIM code [46] to simulate the Gaussian-like ion distribution, we estimated a projected range of $R_P = 38$ nm, a longitudinal straggling of 17 nm and peak concentrations (x_p) ranging from 0.005 to 0.35. Table 1 lists the implanted samples and the corresponding fluences and x_p. All samples were studied in the as-implanted state and after thermal annealing at 800 °C in N_2 flow for 2.5 h, using a GaN proximity cap to minimize surface degradation. In order to avoid sample contamination with ferromagnetic impurities [15], the implantations were carried out using a Mo sample holder and the samples were placed in a ceramic boat during annealing. Each entry in table 1 corresponds to two samples, one for the structural characterization and the other for magnetometry measurements. The samples reserved for the magnetic characterization were handled with non-metallic tweezers in order to avoid magnetic contamination [15].

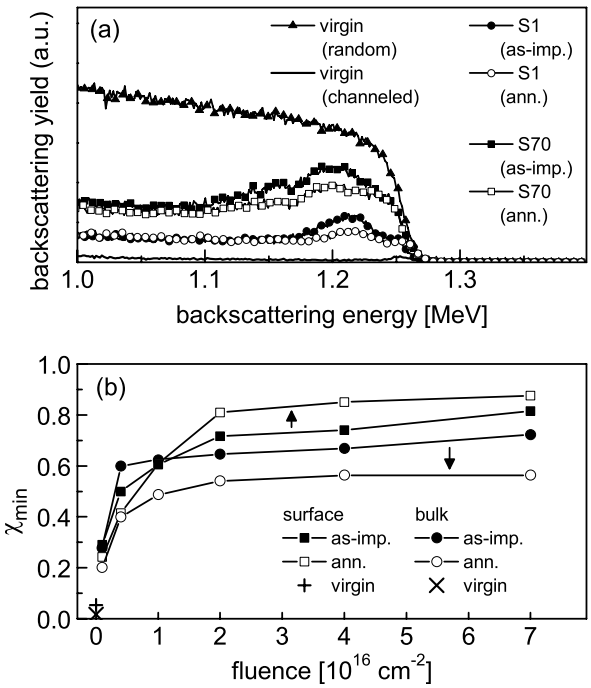

Figure 1. (a) Selected RBS/C spectra: random and channeled spectra of a virgin (unimplanted) GaN sample and channeled spectra of the samples with the lowest (S1, 1×10^{15} cm^{-2}) and the highest (S70, 7×10^{16} cm^{-2}) implanted fluences, before and after annealing at 800 °C. (b) Minimum yield (χ_{min}) determined from both the near-surface and bulk peaks of disorder, before and after annealing, as a function of implanted fluence.

Defect formation and recovery were studied using RBS/C, with a 1.57 MeV He^+ beam. Figure 1 shows examples of spectra obtained in random and channeled geometries (a) and summarizes the results in terms of damage accumulation and recovery in both the near-surface (first few monolayers) and bulk (end of range) regions (b). It is clear that implanting at 300 °C successfully suppresses amorphization, as both near-surface and bulk disorder exhibit saturation at levels which are considerably below the random level. In addition, there is no sign of dramatic surface erosion. This can be inferred from the position of the bulk damage peak relative to the surface. If the film erosion had reached depths of the order of the ion range, the bulk damage peak would have shifted toward the surface as has been reported in [47]. Furthermore, within the experimental uncertainty (<30 nm) the film thickness does not decrease after implantation, even for the maximum fluence. Showing that film erosion was minimal has two important practical consequences. Not only does it show that the nominal Cr content was conserved, it also validates the simulated Cr depth profiles and peak concentrations, calculated assuming a constant film thickness. Regarding the choice of annealing treatment, figure 1 also shows that while providing a significant reduction of the lattice disorder in the Cr-doped region (depicted by the ↓ in figure 1(b)) it kept the near-surface damage peak below random levels.

The possible formation of Cr or CrN precipitates was investigated using conventional XRD. Other than those associated with the GaN layers and the substrate, no additional peaks could be resolved, either before or after annealing (data not shown). Only typical signs of reduced crystalline quality due to implantation were observed. Although thermal annealing of similar wide-gap semiconductors implanted with transition metals can result in the formation of small precipitates which are difficult to detect with conventional XRD (e.g. Co-, Ni- and Fe-implanted ZnO in [18, 19, 17]), Cr was found to be very stable in substitutional sites in GaN, at least up to annealing temperatures of 825 °C [31]. The presence of Cr or CrN precipitates in our samples is thus highly unlikely, both before and after annealing (800 °C). However, although very unlikely in the as-implanted state, the formation of (substitutional) Cr-rich regions during annealing cannot be excluded. Such substitutional clusters would be coherent with the GaN matrix and thus difficult to detect by diffraction techniques. This chemical phase separation by aggregation of the transition-metal dopants, known as spinodal decomposition in the DMS literature, has been observed in a number of DMS materials, including Cr- [44] and Fe-doped GaN [48].

From the structural characterization described in this section we can conclude that, in terms of implantation conditions, we have successfully avoided both amorphization and significant surface erosion. Regarding the annealing treatment, while inducing a significant degree of lattice recovery, we have avoided the formation of secondary phases, at least within the sensitivity of conventional XRD. However, the formation of nanoprecipitates and substitutional Cr clusters cannot be excluded.

2.2. *Magnetic properties*

The magnetic characterization was performed using a superconducting quantum interference device (SQUID) magnetometer (Quantum Design MPMS XL-5) following strict procedures in order to avoid measurement artifacts and external magnetic contributions. These procedures were developed based on statistically relevant tests, which allowed us to determine the practical limits of SQUID magnetometry for the detection of ferromagnetism under various sample preparation, processing and handling conditions [15]. Unless otherwise specified, the measurements shown and discussed below were performed with the field perpendicular to the GaN *c*-axis, i.e. parallel to the film plane.

2.2.1. Absence of ferromagnetic order. A small hysteresis, with a saturation moment always below 1×10^{-6} emu, was observed in some of the samples, up to room temperature. No correlation was found with respect to the fluence or annealing conditions. Since the same residual ferromagnetic-like behavior was observed in unimplanted control samples, we attribute it to small ferromagnetic contaminations [15]. As such, we can conclude the following.

Finding I. None of the samples, regardless of substrate, fluence or annealing treatment, showed ferromagnetic behavior above the range dominated by ferromagnetic contaminations (i.e. with saturation moments $>1 \times 10^{-6}$ emu), from 300 K down to 2 K.

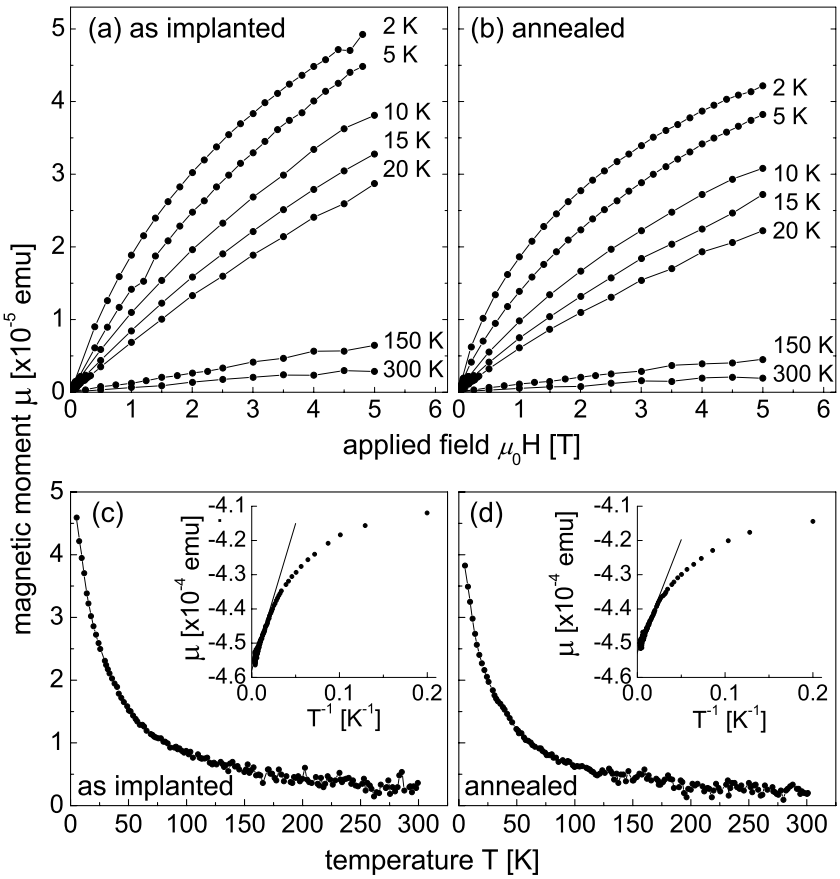

Figure 2. Representative set of SQUID measurements, for sample A70 ($x_p = 0.35$) before ((a) and (c)) and after ((b) and (d)) annealing: *M–H* data ((a) and (b)) at 2, 5, 10, 15, 20, 150 and 300 K and *M–T* data ((c) and (d)) for an applied field of 5 T, all corrected for the diamagnetic background. Insets: uncorrected *M–T* data of (c) and (d) plotted versus T^{-1} with a linear fit between 100 and 300 K.

Since intrinsic irreversibility was not observed in any of the samples, only one quarter of each of the *M–H* loops (magnetization as a function of applied field) is shown in the remainder of this paper, i.e. only the data corresponding to positive and decreasing field.

As a representative example, a typical set of measurements is shown in figure 2 for sample A70 ($x_p = 0.35$) before ((a) and (c)) and after ((b) and (d)) annealing. The magnetic moment (μ) was measured as a function of applied field (*M–H*) up to 5 T at temperatures between 2 and 300 K ((a) and (b)) and as a function of temperature (*M–T*) between 5 and 300 K with an applied field of 5 T ((c) and (d)). All the data in figure 2 are corrected for the diamagnetic component (dominated by the substrate) and exhibit typical paramagnetic behavior. This diamagnetic background was estimated from a linear fit to $\mu(T^{-1})$ above 100 K (insets of (c) and (d)), assuming a Curie behavior of the paramagnetic component and a temperature independent diamagnetic term

$$\chi = \frac{\mu}{H} = \chi_C + \chi_{DM} = \frac{C}{T} + \chi_{DM}, \qquad (1)$$

where χ is the total magnetic susceptibility, χ_C the Curie term, χ_{DM} the diamagnetic term, C the Curie constant and T the temperature. The diamagnetic susceptibility was further corrected by subtracting the very small contribution of ferromagnetic contaminations (when present), estimated from the *M–H* data at 300 K between 2 and 5 T (in saturation). The result was checked for consistency by comparing it with the diamagnetic susceptibility obtained from the linear fit to the *M–H* data at 150 and 300 K, taking into account the paramagnetic component (linear at $T > 100$ K to a good approximation). The Si substrates, both before and after deposition of the GaN thin films, showed a small temperature dependence of χ_{DM}, most likely due to Van Vleck paramagnetism, which has also been observed in other semiconductor substrates, e.g. GaAs [49]. The χ_{DM} value used to correct the *M–H* data of the samples grown on Si was itself corrected for this small temperature dependence, based on measurements of unimplanted samples (as both the diamagnetic and the Van Vleck paramagnetic susceptibilities are extensive properties, i.e. scale with the substrate's mass). We note that, in general, the paramagnetic contribution does not necessarily follow the Curie term in equation (1), but rather a Curie–Weiss law

$$\chi_{CW} = \frac{C}{T - \Theta}, \qquad (2)$$

where Θ is the Weiss constant which accounts for magnetic interactions. Nonetheless, equation (1) holds for $|\Theta/T| \ll 1$, which we show below to be the case in our data. From this point on, all the data that are shown or referred to were corrected for the diamagnetic substrate background

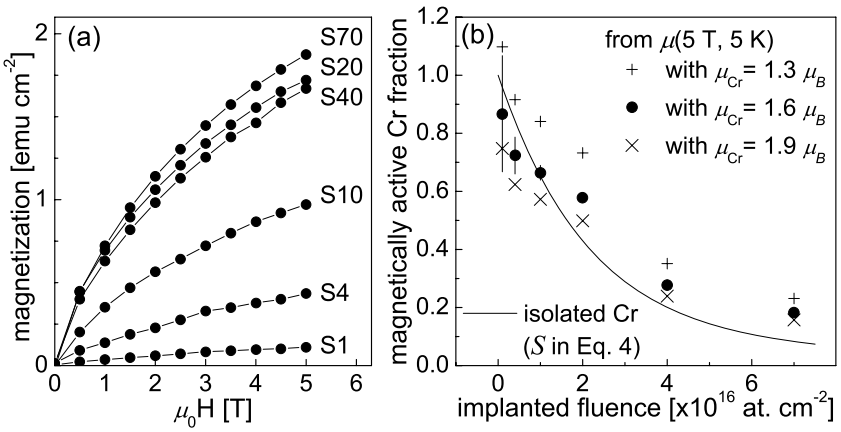

Figure 3. (a) *M–H* at 5 K, in units of emu per unit of the film surface area, after annealing, for the films grown on Si. Note that full saturation is not reached. (b) Fraction of magnetically active Cr atoms, assuming different values of moment per atom (μ_{Cr}) at 5 K and 5 T and fraction of isolated Cr atoms estimated using equation (4) (line), as a function of implanted fluence. The best fit is obtained for $\mu_{Cr} = 1.6\ \mu_B$ (•); the data are also shown for $\mu_{Cr} = 1.3\ \mu_B$ (+) and $\mu_{Cr} = 1.9\ \mu_B$ (×) for comparison. Note that $\mu_{Cr} = 1.6\ \mu_B$ is the non-saturated moment per Cr atom (at 5 K and 5 T).

using this method. This was found to be more accurate than, for example, subtracting *M–H* data measured prior to implantation. Small differences in sample mounting can result in a change of a few per cent in the total measured moment. Since the diamagnetic signal largely dominates, the curves resulting from this subtraction would be affected by an erroneous linear component. At least qualitatively, all the samples show a behavior similar to that of sample S70 (figure 2). We can thus conclude the following.

Finding II. All samples exhibit paramagnetic behavior.

Before discussing the details of this paramagnetism in terms of field and temperature dependence, we will describe how the effective moment per Cr atom evolves with increasing Cr concentration.

2.2.2. Cr moment quenching with increasing Cr concentration. Figure 3(a) shows the magnetization at 5 K, for the implanted and annealed GaN samples grown on Si (the results are equivalent for the Al_2O_3 series). The magnetization does not increase linearly with Cr concentration; there is a clear saturation for fluences above 2×10^{16} cm^{-2}, which, based on the RBS/C data, cannot be ascribed to a saturation of the Cr content due to film erosion. We attribute this effect to the antiparallel alignment of the magnetic moments of Cr atoms sitting in nearest cation neighbor sites, due to strong antiferromagnetic (AFM) interactions. A similar moment quenching effect has been observed in other DMS systems, e.g. Co-doped ZnO [23, 24]. To model this behavior, we assume that all Cr impurities randomly occupy Ga sites [31, 50, 51] and that only isolated Cr atoms, i.e. without Cr nearest cation neighbors in the Ga sublattice, effectively contribute to the magnetization. The fraction of isolated Cr atoms in the GaN hexagonal lattice (S') can be estimated using Behringer's equation

$$S' = (1 - x)^{12}, \tag{3}$$

where x is the fractional concentration of Cr atoms [52]. Since in implanted samples x is a function of depth l, one must integrate S' over the film thickness as

$$S = \int_0^\infty p(l) S'(l)\, \mathrm{d}l, \tag{4}$$

with

$$p(l) = \frac{x(l)}{\int_0^\infty x(l)\, \mathrm{d}l}, \tag{5}$$

where $x(l)$ is the concentration profile which we have simulated using TRIM. Assuming that each of the magnetically active Cr atoms contributes with a moment μ_{Cr} for a given field and temperature, one can extract the corresponding fraction from the experimental data and compare it to that of isolated Cr estimated using equation (4). Figure 3(b) shows the fraction of magnetically active Cr atoms, using $\mu_{Cr} = 1.6\ \mu_B$ (at 5 K and 5 T), which yields the best fit to equation (4). The agreement is fairly good, particularly considering that μ_{Cr} is the only free parameter. Note that $1.6\ \mu_B$ is the non-saturated moment per Cr atom, which can explain why it is smaller than the expected $3\ \mu_B$ for the high-spin Cr^{3+} ($3d^3$) state, predicted by Hund's rules and by *ab initio* calculations [53]. At high concentration, the model somewhat underestimates the active Cr fraction. This is likely to result from considering the simplest case for which only the isolated Cr atoms contribute to the magnetization. For low concentrations, the majority of the non-isolated Cr atoms are in the form of pairs (dimers). Such a dimer configuration may indeed produce an almost perfect antiparallel alignment of the two magnetic moments. However, for higher concentrations, larger complexes of three and more atoms are formed. For these larger substitutional clusters, particularly those containing an odd number of Co atoms, the quenching of the Cr moment may be less efficient due to frustration effects and the presence of uncompensated moments, which may thus contribute to the measured magnetization. This discussion can be concluded as follows.

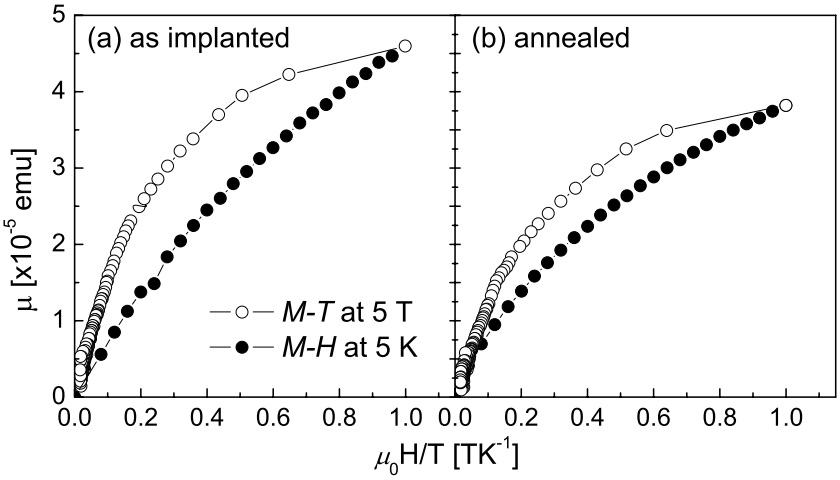

Figure 4. Magnetic moment plotted versus H/T for sample A70 ($x_p = 0.35$) before (a) and after (b) annealing, using M–T data between 5 and 300 K with an applied field of 5 T (○) and M–H data at 5 K up to 5 T (●). As expected, the data do not overlap, i.e. the magnetization does not follow a Brillouin behavior.

Finding III. Strong AFM interactions between the Cr atoms in nearest cation neighbor complexes impose the antiparallel alignment of the corresponding magnetic moments. This results in a Cr moment quenching effect, i.e. a decrease of the effective moment per Cr atom with increasing Cr concentration.

2.2.3. Paramagnetism. While I, II and III constitute the major findings of this work, it is worth discussing in more detail the paramagnetism of the uncompensated (or not fully compensated) Cr moments in GaN and comparing it to the intensively studied and thus better understood wide-gap DMS materials Mn-doped GaN and Co-doped ZnO.

The magnetization of ideal non-interacting magnetic moments with constant total angular momentum quantum number J in a magnetic field H follows the Brillouin function $B_J(H, T)$. This is obviously not the case for Cr moments in GaN, which are subject to (1) the anisotropic GaN crystal field of the host and, as we have shown above, (2) magnetic interactions. The non-Brillouin behavior of our samples is easily confirmed by plotting the M–H and M–T data together as a function of H/T (figure 4). As expected, contrary to what would happen for an ideal Brillouin paramagnet ($\mu(H, T, J) \propto B_J(H/T)$), the curves do not overlap. In the following, we discuss to what extent we find evidence of both effects, (1) anisotropic crystal field and (2) magnetic interactions, in Cr-implanted GaN.

The most easily observable effect of an anisotropic crystal field (effect (1)) on a paramagnetic 3d moment is the resulting anisotropic magnetization. The trigonal crystal field in the wurtzite structure induces a magnetic anisotropy via the spin–orbit interaction, which can be described by an effective spin Hamiltonian with a zero field splitting constant D and an anisotropic effective g-factor ($g_\parallel$ for parallel and $g_\perp$ for perpendicular magnetic field with respect to the c-axis). A strongly anisotropic magnetization was observed, for example, for Mn^{3+} ions in GaN [20] and Co^{2+} ions in ZnO [21], and successfully described by well-established values of the phenomenological parameters D, $g_\parallel$ and $g_\perp$ [21] or more detailed Hamiltonians [20]. Figure 5 shows M–H and M–T data of sample A70 ($x_p = 0.35$) for field applied parallel and perpendicular to the sample plane, i.e. perpendicular and parallel to the GaN c-axis, respectively. Although some degree of anisotropy can be resolved, the effect is much weaker than those observed in Mn-doped GaN [20] and Co-doped ZnO [21]. Because the parameters D, $g_\parallel$ and $g_\perp$ have never been determined for Cr impurities in GaN or similar materials, one cannot predict the magnetic anisotropy for Cr-doped GaN under these experimental conditions. Nonetheless, the fact that the effect is so small in our samples can be explained, at least partially, by the significant disorder induced by implantation (section 2.1), which disturbs the crystal periodicity and consequently the crystal field anisotropy.

In general, the presence of magnetic interactions (effect (2)) can be inferred from magnetization data as a perturbation to the paramagnetic behavior above the associated ordering temperature. In principle, this can be modeled using an effective temperature ($T - \Theta$) where Θ accounts for the magnetic interactions [54], which has been done, for example, for Mn-doped GaN [22] and Co-doped ZnO [24–26]. Applying a similar approach to our data, figure 6 shows the $\mu^{-1}(T)$ data of sample A70 ($x_p = 0.35$) before and after annealing and a fit to the Curie–Weiss law equation (2), which corresponds to the Curie law with an effective temperature $T-\Theta$. The data were fitted only between 60 and 100 K to avoid a possible contribution from frozen O_2 between 30 and 60 K and the large data dispersion above 100 K. The fit yields a negative Θ, $-15(3)$ K and $-5(3)$ K before and after annealing, respectively, which can in principle be interpreted as a signature of AFM interactions. We note, however, that this type of analysis should be applied very carefully. In [21] it is shown that, while the paramagnetism of Co-doped ZnO is correctly modeled using an adequate effective spin Hamiltonian without considering magnetic interactions, attempting to fit the same data using inadequate models such as the Brillouin function or the

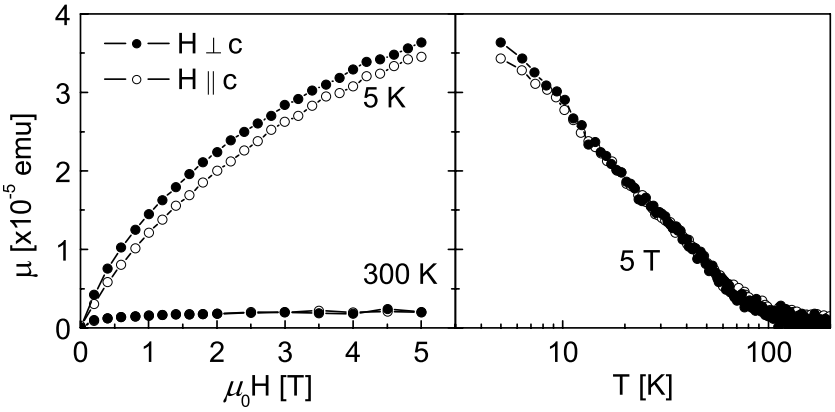

Figure 5. Comparison of the measured magnetization of sample S70 ($x_p = 0.35$), after annealing, for magnetic field applied perpendicular (•) and parallel (○) to the GaN *c*-axis: (a) *M–H* data at 5 K; (b) *M–T* data with an applied field of 5 T.

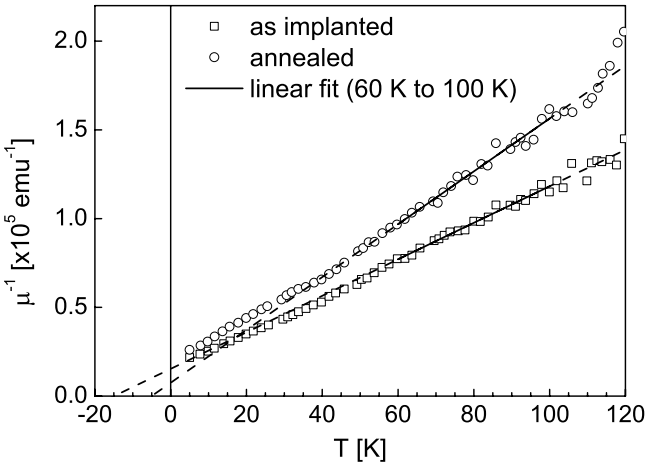

Figure 6. $\mu^{-1}(T)$ data of sample A70 ($x_p = 0.35$) before and after annealing and a Curie–Weiss fit after equation (2) between 60 and 100 K (line). The results of the fit are discussed in the text in terms of AFM interactions and crystal field effects.

Curie law would require the use of an effective temperature $T - \Theta$ ($T + T_0$ in [21]), which could be misinterpreted as an effect of antiferromagnetic interactions. Nevertheless, in our case, because some of the Cr atoms in nearest cation neighbor complexes are not fully compensated, i.e. have a finite contribution to the magnetization (section 2.2.2), it is reasonable to conclude that Θ contains at least a contribution from the nearest cation neighbor AFM interactions.

Finally we will briefly discuss the effect of thermal annealing on the magnetic behavior. We have shown in figure 6 that $|\Theta|$ decreases from $-15(3)$ to $-5(3)$ K upon thermal annealing, indicating a change in crystal field (1) or a weakening of the AFM interactions (2) or a combination of both. The changes in magnetic behavior induced by thermal annealing are even more evident in the *M–H* data. This is illustrated in figure 7 where we show the 5, 20 and 300 K *M–H* data for samples S20 ($x_p = 0.10$) and A70 ($x_p = 0.35$): consistently throughout the entire concentration range, thermal annealing reduces the magnetization, except for very low temperatures and fields where it does the opposite. Structurally, the annealing can have two effects which may explain these changes in magnetic behavior.

(i) Annealing of lattice defects as demonstrated by RBS/C above. Lattice defects in the vicinity of Cr atoms modify the crystal field (1) and may even mediate magnetic

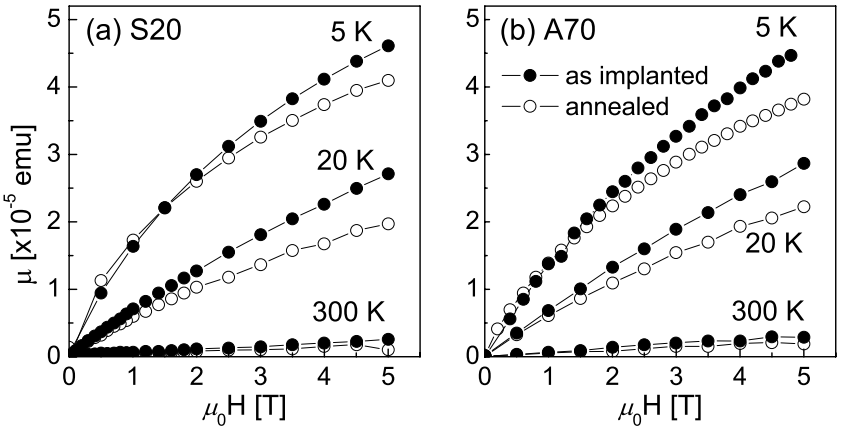

Figure 7. *M–H* data at 5, 20 and 300 K for samples S20 ($x_p = 0.10$) (a) and A70 ($x_p = 0.35$) (b), before (•) and after (○) annealing.

interactions between distant Cr moments (2). Some point defects may even contribute to the magnetization directly. For example, it has been predicted that Ga vacancies induce non-vanishing magnetic moments in the neighboring N atoms [55] and that N vacancies enhance the magnetic moment of isolated Cr impurities [53, 56].

(ii) Aggregation of Cr atoms in substitutional clusters or in small precipitates of Cr or CrN which may be undetectable by XRD. By modifying the dopant spatial distribution, i.e. the relative distance between Cr atoms and the local arrangement of their neighbors, Cr aggregation would also affect the crystal fields (1) and the magnetic interactions (2).

In short, thermal annealing can induce two distinct structural modifications ((i) and (ii)), each of which can modify each of the two parameters which control the magnetic behavior ((1) and (2)). Such an intricate interplay complicates a more quantitative approach to this discussion, which we thus simply conclude as follows.

Finding IV. Uncompensated Cr atoms behave as paramagnetic moments perturbed by AFM interactions in an anisotropic crystal field. Although minimally, thermal annealing affects this paramagnetism, possibly due to an interplay between defect annealing and Cr aggregation.

3. Discussion

The main finding of this study is that the magnetic interactions between Cr moments in GaN are not ferromagnetic but AFM, which is in contrast with previous experimental reports of ferromagnetic order in Cr-doped GaN, e.g. [27–31] for Cr incorporated during growth and [32, 33] for implanted Cr. This is, however, not unexpected. The literature of the last ten years on more extensively studied DMS materials, e.g. Mn-doped GaN, experienced a similar evolution. Despite the many theoretical predictions and experimental reports of high-temperature ferromagnetism, recent studies did not show any indication of high-temperature ferromagnetic order in single-phase Mn-doped GaN [11, 20, 22]. In fact, it is worthwhile discussing in more detail these two cases, Cr- and Mn-doped GaN, together. Two types of magnetic behavior have been comprehensively demonstrated in single-phase Mn-doped GaN: short-ranged AFM interactions between Mn^{2+} ($3d^5$) moments [22] and ferromagnetic order of Mn^{3+} ($3d^4$) moments with a Curie temperature below 10 K [11]. The latter only occurs under stringent growth conditions to ensure epitaxial growth and, most importantly, to minimize the formation of compensating defects such as N vacancy donors [11]. However, because the Mn 3+/2+ acceptor level is deep in the GaN bandgap, the associated holes are strongly localized. Since the coupling between distant moments via *p–d* Zener exchange [57] requires itinerant holes, the observed Curie temperatures are very low (<10 K). More commonly, such stringent growth conditions are not satisfied and compensating donor defects are formed. The Mn impurities are thus incorporated as compensated Mn^{2+} and the *p–d* Zener model does not apply. Consequently, only nearest cation neighbor AFM interactions are observed [22], which are likely to result from indirect superexchange between the Mn 3*d* moments mediated by the N 2*p* band. Indeed, significant hybridization of the Mn 3*d* and N 2*p* states has been observed [58]. This understanding of the magnetic interactions between Mn impurities in GaN in different charge states provides a good framework to interpret our results in the Cr-doping case. Chromium is incorporated in GaN as Cr^{3+} ($3d^3$) [50, 51], with only a donor level (3+/4+) in the bandgap [59]. In the absence of p-holes to mediate *p–d* Zener exchange, our results show that the magnetic behavior of Cr^{3+} ($3d^3$) is very similar to that of Mn^{2+} ($3d^5$): short-ranged AFM interactions, which, as for Mn^{2+}, are likely to result from indirect superexchange mediated by the N 2*p* band. Indeed, the necessary hybridization of the Cr 3*d* and N 2*p* states has also been observed [51, 50].

As an alternative to the *p–d* Zener models discussed in the previous paragraph, high-temperature ferromagnetism in wide-gap DMS materials has also been predicted on the basis of bound magnetic polaron (BMP) models [35]. Here, the magnetic moments interact via electrons associated with a defect impurity band. Since these defect electrons occupy large orbits, each defect can interact with several dopant moments and form a magnetic polaron. Ferromagnetism results from the percolation of such polarons. However, the exchange energy density necessary to produce high-temperature ferromagnetism at a few per cent doping corresponds to a magnetic exchange much stronger than that observed in the strongest of the known ferromagnetic materials [36]. One can thus expect that the critical temperatures associated with this type of magnetic order are well below room temperature.

Our results support the view that the source of high-temperature ferromagnetism often observed in transition-metal-doped GaN may be non-intrinsic, i.e. associated with ferromagnetic precipitates or contaminations. This is in line with a very recent overview of the last ten years of DMS research, which concluded that little proof has been found of high-temperature ferromagnetism in wide-gap DMS materials [1].

4. Conclusions

In summary, we have experimentally demonstrated the absence of ferromagnetic order in Cr-implanted GaN, from 300 K down to 2 K, for Cr fractional concentrations between 0.005 and 0.35. We have shown that the magnetic interactions between Cr moments in GaN are, in fact, AFM. Strong AFM interactions between the Cr atoms in nearest cation neighbor complexes result in Cr moment quenching (compensation), i.e. a decrease of the effective moment per Cr atom, with increasing concentration. Uncompensated Cr atoms behave as paramagnetic moments perturbed by AFM interactions in an anisotropic crystal field. Although minimally, thermal annealing affects the magnetic behavior, possibly due to an interplay between defect annealing and Cr aggregation.

These results suggest that neither type of model of ferromagnetism proposed for dilute magnetic semiconductors, i.e. *p–d* Zener exchange or BMPs, operates in Cr-implanted GaN. Together with recent reports on well-characterized Mn-doped GaN, our study supports the view that the high-temperature ferromagnetism observed in transition-metal-doped GaN may be non-intrinsic.

Acknowledgments

This work was supported by the Research Foundation—Flanders (FWO), the SPIRIT (Support of Public and Industrial Research using Ion Beam Technology) project (contract no. 227012), KULeuven projects GOA/2009/006 and INPAC EF/05/005 and the IUAP P6/42 program. L M C Pereira acknowledges the scholarship SFRH/BD/35761/2007 granted by the Portuguese Foundation for Science and Technology (FCT). T Som acknowledges the FWO for a fellowship.

References

[1] Dietl T 2010 *Nature Mater.* **9** 965
[2] Matsumoto Y, Murakami M, Shono T, Hasegawa T, Fukumura T, Kawasaki M, Ahmet P, Chikyow T, Koshihara S and Koinuma H 2001 *Science* **291** 854
[3] Pearton S J, Abernathy C R, Norton D P, Hebard A F, Park Y D, Boatner L A and Budai J D 2003 *Mater. Sci. Eng.* R **40** 137
[4] Prellier W, Fouchet A and Mercey B 2003 *J. Phys.: Condens. Matter* **15** R1583
[5] Pearton S J, Heo W H, Ivill M, Norton D P and Steiner T 2004 *Semicond. Sci. Technol.* **19** R59
[6] Liu C, Yun F and Morkoc H 2005 *J. Mater. Sci., Mater. Electron.* **16** 555
[7] Dhar S, Brandt O, Ramsteiner M, Sapega V F and Ploog K H 2005 *Phys. Rev. Lett.* **94** 037205
[8] Pan H, Yi J B, Shen L, Wu R Q, Yang J H, Lin J Y, Feng Y P, Ding J, Van L H and Yin J H 2007 *Phys. Rev. Lett.* **99** 127201
[9] Venkatesan M, Fitzgerald C B and Coey J M D 2004 *Nature* **430** 630
[10] Kittilstved K R, Liu W K and Gamelin D R 2006 *Nature Mater.* **5** 291
[11] Sarigiannidou E, Wilhelm F, Monroy E, Galera R M, Bellet-Amalric E, Rogalev A, Goulon J, Cibert J and Mariette H 2006 *Phys. Rev.* B **74** 041306
[12] Abraham D W, Frank M M and Guha S 2005 *Appl. Phys. Lett.* **87** 252502
[13] Ney A, Kammermeier T, Ney V, Ollefs K and Ye S 2008 *J. Magn. Magn. Mater.* **320** 3341
[14] Garcia M A, Fernandez Pinel E, de la Venta J, Quesada A, Bouzas V, Fernandez J F, Romero J J, Martin Gonzalez M S and Costa-Kramer J L 2009 *J. Appl. Phys.* **105** 013925
[15] Pereira L M C, Araujo J P, Van Bael M J, Temst K and Vantomme A 2011 *J. Phys. D: Appl. Phys.* **44** 215001
[16] Sun Z, Yan W, Zhang G, Oyanagi H, Wu Z, Liu Q, Wu W, Shi T, Pan Z, Xu P and Wei S 2008 *Phys. Rev.* B **77** 245208
[17] Zhou S *et al* 2008 *J. Appl. Phys.* **103** 023902
[18] Zhou S, Potzger K, von Borany J, Grotzschel R, Skorupa W, Helm M and Fassbender J 2008 *Phys. Rev.* B **77** 035209
[19] Zhou S, Potzger K, Kuepper K, Grenzer J, Helm M, Fassbender J, Arenholz E and Denlinger J D 2008 *J. Appl. Phys.* **103** 043901
[20] Stefanowicz W *et al* 2010 *Phys. Rev.* B **81** 235210
[21] Ney A, Kammermeier T, Ollefs K, Ye S, Ney V, Kaspar T C, Chambers S A, Wilhelm F and Rogalev A 2010 *Phys. Rev.* B **81** 054420
[22] Granville S, Ruck B J, Budde F, Trodahl H J and Williams G V M 2010 *Phys. Rev.* B **81** 184425
[23] Ney A, Ollefs K, Ye S, Kammermeier T, Ney V, Kaspar T C, Chambers S A, Wilhelm F and Rogalev A 2008 *Phys. Rev. Lett.* **100** 157201
[24] Sati P, Deparis C, Morhain C, Schafer S and Stepanov A 2007 *Phys. Rev. Lett.* **98** 137204
[25] Xu Q *et al* 2009 *J. Phys. D: Appl. Phys.* **42** 085001
[26] de Carvalho H B *et al* 2010 *J. Appl. Phys.* **108** 033914
[27] Hashimoto M, Zhou Y K, Kanamura M and Asahi H 2002 *Solid State Commun.* **122** 37
[28] Park S E, Lee H J, Cho Y C, Jeong S Y, Cho C R and Cho S 2002 *Appl. Phys. Lett.* **80** 4187
[29] Zhou Y K, Hashimoto M, Kanamura M and Asahi H 2003 *J. Supercond.* **16** 37
[30] Kim J J, Makino H, Sakurai M, Oh D C, Hanada T, Cho M W, Yao T, Emura S and Kobayashi K 2005 *J. Vac. Sci. Technol.* B **23** 1308
[31] Singh R K, Wu S Y, Liu H X, Gu L, Smith D J and Newman N 2005 *Appl. Phys. Lett.* **86** 012504
[32] Lee J S, Lim J D, Khim Z G, Park Y D, Pearton S J and Chu S N G 2003 *J. Appl. Phys.* **93** 4512
[33] Wang J Q, Chen P P, Guo X G, Li Z F and Lu W 2005 *J. Cryst. Growth* **275** 393
[34] Pipeleers B, Hogg S M and Vantomme A 2005 *J. Appl. Phys.* **98** 123504
[35] Coey J M D, Venkatesan M and Fitzgerald C B 2005 *Nature Mater.* **4** 173
[36] Coey J M D, Stamenov P, Gunning R D, Venkatesan M and Paul K 2010 *New J. Phys.* **12** 053025
[37] Wang M J, Yuan L, Cheng C C, Beling C D and Chen K J 2009 *Appl. Phys. Lett.* **94** 061910
[38] Kucheyev S O, Williams J S, Jagadish C, Zou J and Li G 2000 *Phys. Rev.* B **62** 7510
[39] Vantomme A *et al* 2001 *Nucl. Instrum. Methods Phys. Res.* B **175** 148
[40] Jiang W and Weber W J 2006 *Nucl. Instrum. Methods Phys. Res.* B **242** 431
[41] Kucheyev S O, Williams J S, Zou J, Jagadish C and Li G 2001 *Appl. Phys. Lett.* **78** 1373
[42] Vanvecht J A 1973 *Phys. Rev.* B **7** 1479
[43] Williams J S 1998 *Mater. Sci. Eng.* A **253** 8
[44] Gu L, Wu S Y, Liu H X, Singh R K, Newman N and Smith D J 2005 *J. Magn. Magn. Mater.* **290** 1395
[45] Nord J, Nordlund K, Pipeleers B and Vantomme A 2003 *Mater. Sci. Eng.* B **105** 111
[46] Biersack J P and Haggmark L 1980 *Nucl. Instrum. Methods* **174** 257
[47] Kucheyev S O, Williams J S, Zou J, Jagadish C and Li G 2001 *Nucl. Instrum. Methods Phys. Res.* B **175** 214
[48] Bonanni A *et al* 2008 *Phys. Rev. Lett.* **101** 135502
[49] Ney A, Harris Jr J S and Parkin S S P 2006 *J. Phys.: Condens. Matter* **18** 4397
[50] Takeuchi T *et al* 2004 *Phys. Rev.* B **70** 245323
[51] Hashimoto M, Emura S, Tanaka H, Honma T, Umesaki N, Hasegawa S and Asahi H 2006 *J. Appl. Phys.* **100** 103907
[52] Behringer R E 1958 *J. Chem. Phys.* **29** 537
[53] Cui X Y, Medvedeva J E, Delley B, Freeman A J and Stampfl C 2007 *Phys. Rev.* B **75** 155205
[54] Buschow K H J and De Boer F R 2004 *Physics of Magnetism and Magnetic Materials* (New York: Kluwer) p 24
[55] Hong J 2008 *J. Appl. Phys.* **103** 063907
[56] Xu B and Pan B C 2009 *J. Appl. Phys.* **105** 103710
[57] Dietl T, Ohno H, Matsukura F, Cibert J and Ferrand D 2000 *Science* **287** 1019
[58] Wang D, Zhang X, Wang J and Koide T 2009 *Solid State Commun.* **149** 192
[59] Gerstmann U, Blumenau A T and Overhof H 2001 *Phys. Rev.* B **63** 075204